PROCEEDINGS, 51st Workshop on Geothermal Reservoir Engineering
Stanford University, Stanford, California, February 9-11, 2026
SGP-TR-230

Non-clinkered Calcium Carbonate Based Cementitious Composites for Enhanced Geothermal Systems (EGS)

Tatiana Pyatina[1)], Michelle Devoe[1)], Sizhan Liu[1)], Jianming Bai[2)]

[1]Interdisciplinary Science Department, Brookhaven National Laboratory, Upton, New York 11973, United States

[2]National Synchrotron Light Source II, Brookhaven National Laboratory, Upton, New York 11973, United States

tpyatina@bnl.gov, jmbai@bnl.gov

Keywords: High-temperature geothermal cement; non-clinkered cement; alkali activation; calcium–silicate binders; phase assemblage; hydrothermal curing

ABSTRACT

Reliable cementing solutions are critical for high-temperature geothermal wells, yet current technologies rely on clinkered Ordinary Portland Cement (OPC) or costly Calcium Aluminate Cement (CAC) systems with limited economic and environmental sustainability. This work presents a distinct, non-clinkered alternative that reconstitutes calcium-silicate binding chemistries relevant to geothermal well cementing from low-cost mineral precursors. A calcium carbonate-silica-olivine system activated under hydrothermal conditions was systematically designed and evaluated to elucidate the roles of precursor composition, activator chemistry, and phase evolution on mechanical performance at 300 °C.

Unconfined compressive strength and water-fillable porosity were measured as functions of activator concentration, curing time, and mineral replacement. Sodium metasilicate was found to control early activation kinetics through competitive dissolution of calcium carbonate, olivine and silicate phases, resulting in non-monotonic relationships between strength and porosity. Silica flour acted as a latent silicate source, sustaining binder formation at later ages, while partial replacement of calcium carbonate with olivine provided a rigid structural backbone and a delayed magnesium source, increasing compressive strength to above 2000 psi. Addition of sodium bicarbonate further enhanced sodium availability and phase stability, producing compressive strengths exceeding 3000 psi within 21 days of curing.

Crystalline phase analysis revealed that activator selection governs reaction pathways and phase assemblages, with sodium bicarbonate acting as a strong phase-directing agent that accelerates kinetics and shifts calcium-sodium silicate formation from transitional lalondeite to the more stable pectolite phase. Mechanical performance was shown to depend primarily on phase assemblage, crystallinity, and interfacial bonding rather than total porosity alone. The results demonstrate that economically viable, non-clinkered mineral systems can be chemically designed to achieve mechanical performance consistent with geothermal cementing requirements while following fundamentally different pathways from previously explored high-temperature cement alternatives.

1. INTRODUCTION

Competent cementing solutions are critical for high-temperature (HT) geothermal wells, as cement failure can result in costly repairs, redrilling, or well abandonment. Currently deployed geothermal well cements are largely limited to conventional Ordinary Portland Cement (OPC)-based blends, which exhibit limited chemical stability at elevated temperatures (Pyatina et al., 2024), or to chemically stable but costly calcium aluminate cement (CAC) systems (Arbad et al., 2022; Bergen et al., 2022). Despite decades of research and development, alternative cementitious solutions proposed for HT geothermal applications, including blended supplementary cementitious materials and so-called geopolymer systems (Devers, Romero Tellez, et al., 2022; Devers, Teodoriu, et al., 2022; Ranjbar & Zhang, 2020), that have largely relied on chemistries fundamentally different from OPC, have not displaced existing technologies. Moreover, all of these systems depend on clinkered or high-temperature-processed starting materials, contributing to high material cost and environmental impact.

Identifying and validating economical, non-clinkered cementitious materials that retain the advantageous calcium–silicate binding chemistry familiar from OPC, while avoiding clinker production, would therefore provide substantial technical and economic benefits to the geothermal industry. Prior efforts to move beyond traditional cement formulations have demonstrated the feasibility of designing high-performance composites from alternative precursors (Liu, Devoe, Samuel, et al., 2025; Liu, Devoe, Sugama, et al., 2025). These studies predominantly explored distinct chemical pathways to design aluminum-rich chemistries for applications under highly acidic conditions rather than reconstituting calcium–silicate binders from non-clinkered sources under geothermal conditions.

In this context, calcium carbonate along with other natural rocks (Smalakyas, 2021) represents an attractive non-clinkered precursor due to its wide availability, low cost, and ability to supply calcium for cementitious phase assemblages analogous to those in OPC systems. Under elevated geothermal temperatures and alkali activation, calcium carbonate dissolution can be significantly accelerated, increasing calcium availability in solution. A highly soluble alkaline silicate activator provides an immediate source of silicate ions, enabling rapid formation of binding calcium silicates, while a latent silica source, such as silica flour already widely used in HT geothermal cementing, supports continued binder evolution, reinforcement, and long-term thermal stability.

Additional system design is required to ensure long-term performance through controlled phase evolution under hydrothermal conditions. In this work, the system is deliberately formulated with the understanding that early-forming sacrificial phases and elemental redistribution may occur, provided that mechanical performance is maintained, and the assemblage evolves toward more thermodynamically stable products. Initial performance targets include relatively rapid compressive strength development on the order of approximately 1000 psi, low water-fillable porosity (below ~50%), and phase assemblages reasonably expected to remain stable under the EGS conditions.

High-temperature geothermal well cements are inherently multicomponent systems in which mechanical performance arises from interactions among multiple solid phases rather than from isolated single-phase reactions. Accordingly, this study adopts a design-driven approach that begins with a deliberately complex, application-relevant formulation comprising calcium carbonate, silica, olivine, and alkaline activators. Each component serves a distinct functional role, such as calcium supply, latent silicate availability, structural reinforcement, and kinetic/phase control. Their combined behavior under hydrothermal conditions determines overall performance. By systematically modifying individual components and activator concentrations within this multicomponent framework, mechanistic insights into phase evolution and property development are extracted while maintaining relevance to geothermal cementing applications.

This paper presents an economic, non-clinkered calcium carbonate-silica-olivine cementitious system with sodium metasilicate (Na_2SiO_3, SMS) and sodium bicarbonate ($NaHCO_3$, SBC) activators, correlating mechanical and physical property evolution with crystalline phase analysis under hydrothermal curing at 300 °C. The key contribution of this work is the demonstration that mechanically robust binding behavior relevant to geothermal well cementing can be achieved from low-cost, non-clinkered mineral precursors through chemically designed activation pathways that promote calcium–silicate–involving reaction chemistry under hydrothermal conditions.

2. MATERIALS AND METHODS

Dry blends were prepared with calcium carbonate, CC (Imerfill 50-M, supplied by Imerys), silica flour, Si (supplied by Spinnaker cementing solutions), olivine, OLV (RePlug, supplied by ReStone AS), sodium metasilicate from PQ Corporation (MetsoBeads 2048), and sodium bicarbonate from Sigma Aldrich.

Table 1 shows crystalline compositions of calcium carbonate and olivine precursors. Phase fractions were determined by X-ray diffraction with Rietveld refinement. Iron substitution in olivine-group and chlorite phases cannot be fully excluded by XRD and phases are treated as Mg-endmembers for stoichiometric analyses. The absence of the amorphous fraction in calcium carbonate was determined with the internal standard of Al_2O_3 additions.

Table 1: Crystalline compositions of olivine and calcium carbonate precursors.

Precursor material	Phase	Chemical formula (idealized)	Weight fraction (wt.%)
Olivine (OLV) (RePlug, ReStone AS)	Forsterite	Mg_2SiO_4	77.70
	Enstatite	$MgSiO_3$	8.13
	Antigorite	$Mg_3Si_2O_5(OH)_4$	4.77
	Chlorite	$(Mg,Fe)_5Al(Si_3Al)O_{10}(OH)_8$	4.46
	Talc-1A	$Mg_3Si_4O_{10}(OH)_2$	2.98
	Quartz	SiO_2	1.95
	Subtotal	—	100.00
Calcium carbonate (CC) (Imerfill 50-M, Imerys)	Calcite	$CaCO_3$	~100
	Dolomite	$CaMg(CO_3)_2$	trace
	Amorphous	—	not detected

The experimental workflow comprised (i) dry-blend preparation of the reactants, (ii) room-temperature mixing with water to form a slurry, (iii) hydrothermal curing, and (iv) characterization by XRD, mechanical testing, and water-fillable porosity measurements. All dry components of each tested dry blend were first homogenized by vigorous shaking for 3 minutes. Deionized water was then added to each dry blend in quantities sufficient to achieve comparable self-leveling slurry consistency across all formulations. For the final blends, that included calcium carbonate (CC), silica (Si), and olivine (OLV), the water-to-blend (CC/Si/OLV) ratio was 0.32 for all concentrations of SBC activator and 10% by weight of blend SMS. The slurries were manually stirred for an additional 3 minutes. The resulting slurry was then poured into a mold and left for 24 hours at ambient temperature, allowing the hydrolysis of SMS in the slurry to begin. The slurry-filled mold was placed in a 99 ± 1% relative humidity chamber for 24 hours at 85°C. Subsequently, demolded samples were autoclaved in the Parr Reactor model 4622 and 4680 (Hillsboro, OR, USA) at 300 °C for 1, 7, 14 and 21 days at 1200 psi pressure. The heating rates

for the autoclaves were approximately 115-120°C/h. This procedure loosely mimicked slurry preparation for geothermal cementing, where slurries are mixed at room temperature, then pumped into a well cooled with the circulating fluids with the temperature increasing to the static well temperature.

Table 2 shows the base blend composition used in the CC/Si/OLV systems.

Table 2: Base blend composition (dry solids excluding water).

Component	Weight fraction (wt.%)
Calcium carbonate	36
Silica flour	24
Olivine	40
Total	100

SMS: 10wt.% relative to the base blend; SBC: 0-7 wt.% relative to the base blend.

Phase composition analysis was conducted using X-ray diffraction and Rietveld refinement. Synchrotron X-ray diffraction (XRD) was performed at beamline 28-ID-2 of the National Synchrotron Light Source II (NSLS-II), Brookhaven National Laboratory (BNL). The incident X-ray beam had a wavelength of 0.1841 Å with a spot size of 0.5 mm × 0.5 mm at the sample position. A Perkin-Elmer XRD 1621 digital imaging detector, positioned approximately 1400 mm from the sample, was used to collect the diffraction patterns. The 2D diffraction images were integrated into a 1D xy dataset using the *Dioptas* software (Prescher & Prakapenka, 2015). A mask was applied prior to integration to remove contributions from dead pixels and the beamstop shadow.

Phase identification was carried out using the PDF-5+ 2025 database (International Centre for Diffraction Data, ICDD) and the Crystallographic Open Database (COD). Quantitative phase analysis was performed using *TOPAS-Academic V7.12 (Coelho, 2018).* The refined parameters included background coefficients, zero-shift, peak shape parameters, lattice parameters, and phase fractions. Atomic coordinates (XYZ) and isotropic atomic displacement parameters (Beq) were held fixed to prevent overfitting. Corrections for preferred orientation were not applied because no indications of preferred orientation, such as poor intensity fit, were observed in the major phases. It is possible that preferred orientation is present in the minor phases, however applying correction functions led to overfitting and was therefore omitted. The quality of the Rietveld refinement was evaluated using the weighted profile R-factor (Rwp) (Coelho, 2018).

The mechanical properties, including compressive strength, Young's Modulus, and compressive fracture toughness, as a function of SMS content and hydrothermal temperature for cylindrical cement samples (20 mm diameter × 40 mm) were determined using an Electromechanical Instron System Model 5967. The compressive fracture toughness was calculated by measuring the total pre-stress and post-stress energy absorptions consumed until the cement's compressive failure. This was computed from the enclosed area between the beginning and the end of the compressive stress-strain curve.

The water-fillable porosity for water-saturated samples was computed by $(W_{wet}-W_{dry})/V_{vs}\times 100\%$, where W_{wet} is the weight of the water-saturated sample, W_{dry} is the weight of the sample dried for at least four days in vacuum oven at 65 ^{o}C until the sample's weight becomes constant and V_{vs} is the volume of sample.

3. RESULTS AND DISCUSSION

We first present XRD-derived phase evolution, then a stoichiometric mass-balance analysis, and finally mechanical response with integrated interpretation.

3.1 Crystalline phase development

Crystalline compositions of tested systems are shown in Table 3. All the systems were activated with 10% by weight of blend SMS. The blends of calcium carbonate/silica flour/olivine (CC/Si/OLV) had weight percent composition of 36/24/40; the blend of olivine/silica flour (OLV/Si, no CC) had the weight percent composition of 60/40. For all reported formulations, forsterite remains the dominant olivine mineral; however, because the olivine precursor is multiphase, its persistence reflects partial and selective dissolution of Mg-silicate phases rather than incomplete activation of a monomineralic olivine. Crystalline silica primarily reflects residual silica flour, while calcium carbonate fractions include both unreacted precursor and secondary carbonate formed through hydrothermal dissolution–reprecipitation processes. Even moderate addition of SBC noticeably accelerates kinetics of calcium-sodium silicates formation. With 3% SBC, lalondeite decreases from ~6% (1 day) to ~4% (7 days), while pectolite increases; at 7% SBC, lalondeite is ~3% at 1 day but increases to ~8% at 7 days, whereas pectolite increases to >10%. At 1 day, increasing SBC addition from 0% to 7% reduces forsterite content from approximately 16% to 11–13%, reflecting enhanced but still partial dissolution of Mg-silicate phases from the multiphase olivine precursor. This dissolution is promoted by increased alkalinity and sodium availability rather than by complete olivine breakdown. In contrast, the observed concentrations of calcium carbonate and silica exhibit a modest increase from ~30% to ~40% with increasing SBC content, which may indicate the presence of amorphous phases.

Taken together, the phase fractions in Table 3 indicate that SBC shifts Ca partitioning toward Na-stabilized Ca silicates, while carbonate persistence implies concurrent buffering of dissolved Ca through secondary carbonate precipitation. To translate these phase trends into a chemical picture, we summarize below the dominant pore-solution reactions initiated by SMS hydrolysis and the representative precipitation pathway leading to lalondeite and its evolution toward pectolite. The reactions are intended as simplified representations of coupled dissolution–precipitation processes under hydrothermal curing at 300 °C.

Table 3: Crystalline phases compositions in calcium carbonate, olivine, silica systems activated with SMS and sodium bicarbonate.[1]

Days at 300°C	Forsterite	Silica	Calcium carbonate	Lalondeite	Pectolite	Enstatite	Brucite	Talc-1A	Dolomite	Scawtite	Mg carbonate	Siderite
0% SBC, 10% SMS												
1	16.36	31.35	33.25	13.98	3.41	1.40	0.26	-	-	-	-	-
7	12.90	34.95	36.03	10.52	3.35	0.90	0.36	0.99	-	-	-	-
14	15.72	33.03	33.57	10.44	5.03	0.77	0.39	1.06	-	-	-	-
21	11.81	37.78	31.15	7.94	9.08	0.65	0.42	1.17	-	-	-	-
3% SBC, 10% SMS												
1	14.64	33.60	33.01	6.04	7.59	1.36	-	-	3.75	-	-	-
7	11.43	40.81	33.93	3.87	8.70	1.25	-	-	-	-	-	-
5% SBC, 10% SMS												
1	11.55	42.16	34.79	-	10.55	-	-	0.95	-	-	-	-
7	10.17	42.54	32.37	-	10.44	2.87	0.34	1.26	-	-	-	-
14	11.54	37.75	33.8	-	12.89	1.89	0.46	1.67	-	-	-	-
21	10.79	35.38	30.79	-	16.26	-	-	2.24	-	4.54	-	-
7% SBC, 10% SMS												
1	11.06	39.57	37.39	3.02	7.62	1.34	-	-	-	-	-	-
7	12.79	30.32	31.84	8.10	11.68	5.27	-	-	-	-	-	-
OLV/Silica/10% SMS/5% SBC – no calcium carbonate												
1	39.94	48.76	-	-	-	4.92	1.06	3.25	-	-	1.69	0.37
7	38.70	48.32	-	-	-	4.44	1.31	4.96	-	--	1.93	0.33

The dissolution reaction of highly soluble SMS is:

$Na_2SiO_3+H2O \rightarrow 2Na^+ + OH^- + HSiO_3^-$

The high pH from SMS dissolution promotes partial calcium carbonate dissolution described by the generalized reaction:

[1] Reported phase abundances reflect the combined presence of unreacted precursor minerals and reaction-derived phases. The olivine precursor is multiphase, consisting primarily of forsterite (77.70 wt%) with minor enstatite, antigorite, chlorite, talc-1A, and SiO_2; therefore, persistence of Mg-silicate phases indicates partial and selective dissolution rather than complete olivine transformation. Calcium carbonate fractions include both unreacted precursor and secondary carbonate formed via dissolution–reprecipitation under alkaline hydrothermal conditions. Dolomite has also been detected in the calcium carbonate precursor.

$CaCO_3 \rightleftharpoons Ca^{2+} + CO_3^{2-}$

As a result, in addition to dissolved calcium and silicate species from SMS (compositions similar to OPC slurries) in the case of alkali-activated calcium carbonate, the pore solution is strongly alkaline with high sodium content. This leads to formation of Na-bearing calcium silicates in these systems that are further promoted by carbonates, buffering calcium ion activity through precipitation of secondary calcium carbonates. These secondary calcium carbonates can serve as binding low-permeability phases as well.

In the place of tobermorite and xonotlite formation ($5CaO+6SiO_2+5H_2O \rightarrow Ca_5Si_6O_{16}(OH)_2 \cdot 4H_2O$ and $6CaO+6SiO_2+H_2O \rightarrow Ca_6Si_6O_{17}(OH)_2$), observed in OPC systems, the representative reaction pathway becomes:

$4CaCO_3+Na_2SiO_3+5SiO_2+H_2O \rightarrow 2NaCa_2Si_3O_8(OH)+4CO_2$

The sodium–calcium silicates lalondeite and pectolite observed in the studied systems exhibit short, isolated silicate chains, unlike the more polymerized chain and layered frameworks of tobermorite and xonotlite. This structural distinction is consistent with the formation of lalondeite and pectolite in carbonated natural environments (Eslami et al., 2025). Lalondeite is a transitional crystalline phase where xonotlite/tobermorite formation is prevented by high alkali concentrations (Tian et al., 2021). As an intermediate phase lalondeite transitions to pectolite. At elevated temperature water loss leading to free energy decrease is favored. A simplified representation of lalondeite to pectolite transition is:

$NaCa_4Si_5O_{14}(OH) \cdot H_2O+H_2O \rightarrow NaCa_2Si_3O_8(OH)+2Ca^{2+}+2H_2SiO_4^{2-}$

In natural systems, the formation of pectolite is associated with elevated calcium and sodium concentrations and may significantly modify the porosity and permeability of the rock matrix, in contrast to the lighter and more porous structures of synthetic tobermorite or xonotlite (Li et al., 2025). Under the tested conditions at 300 °C, SBC acts as a phase directing agent, shifting the Ca silicate assemblage from lalondeite toward pectolite and accelerating the overall precipitation kinetics, while limiting the persistence of intermediate calcium silicate phases. This phase selection requires a readily available Ca source, and calcium carbonate plays an essential role by supplying Ca for Na-Ca-silicate binder formation. By contrast, in $CaCO_3$-free formulations, non-reacted olivine (forsterite) and silica remain dominant regardless of SBC concentration, with only limited secondary modification and minor carbonate formation, and no mechanically effective Na–Ca-silicate binder develops under the tested conditions. Carbonate derived from SBC preferentially precipitates as magnesium carbonate and minor siderite via reactions with the major olivine phase, forsterite, and its minor iron impurities. In comparison with the calcium rich, calcium carbonate formulations, this system developed limited strength after 300 ^oC curing for 1, 7, 14, and 21 days, with no measurable strength at 1 day and compressive strengths of 650, 1070, and 1330 psi, respectively. The formulation of CC/OLV/Silica activated with 5% SBC without SMS was also slow to develop strength, showing no measurable strength at 1 day and only 500 psi after 7 days of 300 ^oC curing. Together, these results suggest that olivine dissolution is comparatively slow and cannot be sufficiently accelerated by SBC additions alone to produce early mechanical properties, whereas calcium carbonate enables faster Ca availability that supports earlier formation of Na-Ca-silicate binding phases.

3.2 Stoichiometric Analysis of Crystalline Phase Assemblages

To assess elemental redistribution beyond phase identification given in Table 3, we converted the Rietveld-refined crystalline phase fractions into molar inventories of Ca, Si, and Mg using idealized phase stoichiometries. Because Rietveld refinement normalizes phase fractions to the quantified crystalline inventory (i.e., phases detected and included in the refinement), the resulting Ca/Si and Mg/Si ratios reflect elemental partitioning within the identified crystalline phases only. Comparing these crystalline-only ratios with the bulk precursor stoichiometry therefore provides a mass-balance check: systematic deviations indicate that a fraction of an element resides outside the quantified crystalline phases, for example in amorphous or poorly crystalline products, undetected minor phases, or dissolved species.

Across all calcium-carbonate-containing formulations, the crystalline Ca/Si ratios remain close to those expected from the precursor blend composition, ranging from approximately 0.42 to 0.51 depending on activator content and curing time. This agreement indicates that most Ca supplied by calcium carbonate is captured within the quantified crystalline phases (including residual calcite and newly formed Na–Ca silicate phases), and therefore the crystalline Ca/Si ratios do not require substantial Ca incorporation into amorphous or poorly crystalline products to satisfy mass balance. In contrast, the crystalline Mg/Si ratios are systematically lower than those expected from the precursor composition. Whereas the precursor blend exhibits Mg/Si ratios on the order of ~0.7–0.8 (depending on whether activator-derived silica is included), the crystalline assemblages typically yield Mg/Si ratios between ~0.19 and 0.30, and this offset persists across curing times and SBC concentrations. Because Mg is primarily supplied by the multiphase olivine precursor and crystalline Mg-silicate phases (forsterite, enstatite, talc) remain abundant in the reacted materials, bulk Mg loss from the system is unlikely. An alternative interpretation is that a fraction of Mg resides in reaction products that are poorly crystalline, nanocrystalline, or otherwise below conventional X-ray diffraction quantification limits. Possible sinks include fine-grained Mg-silicate materials and mixed Ca–Mg–Si reaction domains associated with particle surfaces, reaction rims, or pore-filling regions. This stoichiometric analysis indicates that some Mg resides outside the quantified crystalline phases, but it cannot determine the exact nature of the low-crystallinity products. This inference is consistent with the observation that strength can evolve even when the crystalline assemblage changes only modestly. The implications for strength development are discussed in the following section.

3.3 Mechanical Properties

Unconfined compressive strength (UCS) and water-fillable porosity results are presented below to evaluate the mechanical consequences of the phase assemblages and stoichiometric redistribution identified in Sections 3.1-3.2. Together, these measurements provide a structure–property perspective on how formulation modifications influence macroscopic performance under hydrothermal conditions.

Figure 1 shows UCS and porosity development in SMS activated calcium carbonate system after a day of autoclaving at 300°C for different SMS concentrations. UCS increases monotonically with SMS concentration, from <100 psi at low SMS to > 400 psi at 10, 12% SMS. On the other hand, water-fillable porosity shows a non-monotonic response: high porosity at low SMS, minimum at 8-10% SMS, slight increase at the highest SMS level. The results imply that SMS acts as an activator controlling dissolution of $CaCO_3$ and formation of reaction products involving calcium and silicate species that contribute to the mechanical performance. Porosity minimization at intermediate SMS levels arises from a balance between dissolution-induced pore generation and solid precipitation within the pore network. However, at high alkalinity increasing porosity can be caused by increased silica-rich gel or crystalline phase formation leading to reopening of pores. Early strength development is therefore governed primarily by activation chemistry rather than by bulk porosity alone. Thus, SMS content introduces a trade-off between porosity and early strength.

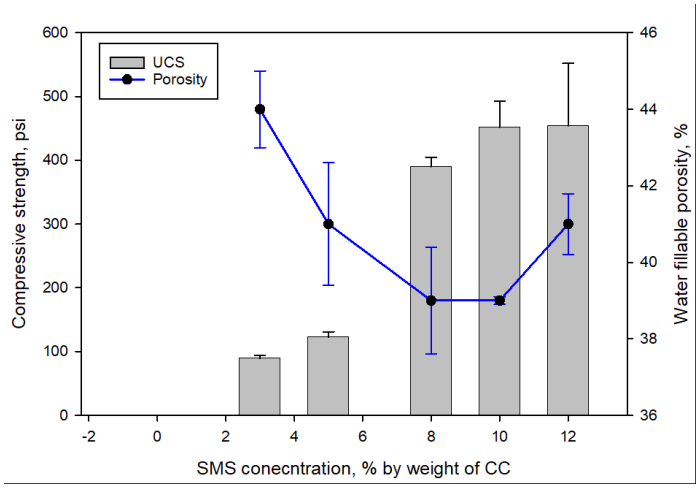

Figure 1: UCS and water-fillable porosity of calcium carbonate samples activated with SMS after one day of autoclave curing at 300°C.

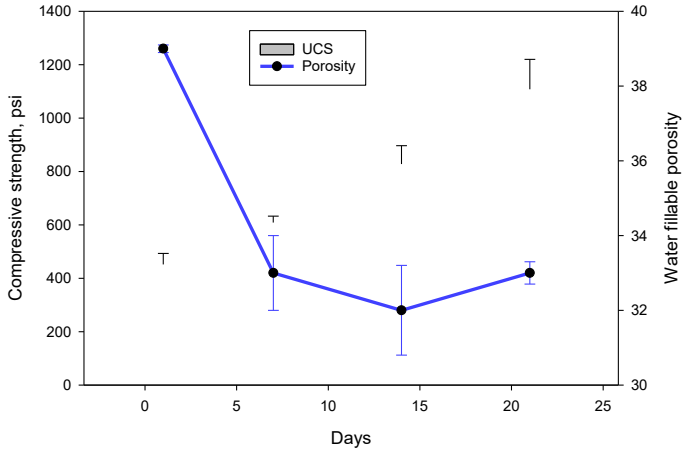

Figure 2: UCS and water-fillable porosity of calcium carbonate samples activated with 10% SMS after different autoclave curing times at 300°C.

UCS increases strongly with curing time (~450 psi to >1100 psi from 1 to 21 days, Figure 2). Porosity drops sharply from day 1 to day 7, then stabilizes or slightly rebounds. Similar to the early UCS, at later stages it is not directly proportional to porosity. This indicates that mechanical performance is increasingly governed by phase assemblage and bonding, not bulk pore volume alone.

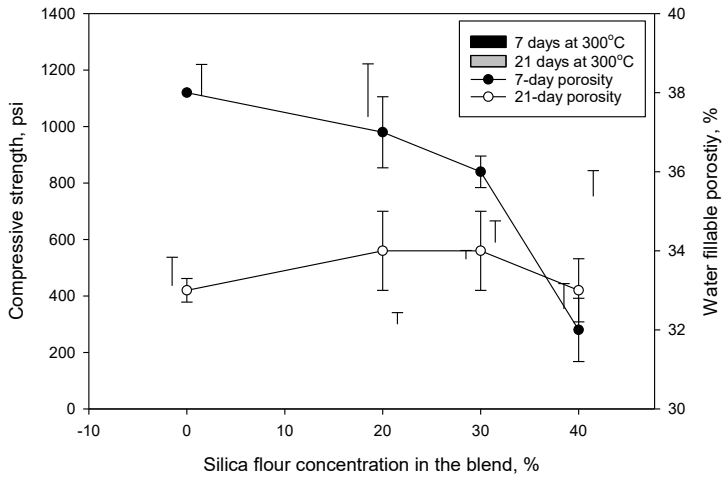

Figure 3: Effect of silica flour content on UCS and water-fillable porosity of calcium carbonate samples activated with 10% by weight of blend SMS after different autoclave curing times at 300°C.

The system containing 10% SMS was further modified by partially replacing calcium carbonate with silica flour to promote longer-term development of silicate-involving binding phases through high-temperature reactions of the silica flour. Silica addition modifies the balance between calcium, silicate, and alkali availability, which is reflected in both crystalline phase evolution and mechanical response. As shown in Figure 3, UCS exhibits a pronounced non-linear dependence on silica content. The silica-free system shows low early strength but substantial strength gain by 21 days, whereas incorporation of 20% silica results in relatively high early-age UCS followed by a pronounced reduction (~75%) in 21-day UCS relative to the silica-free system. This substantial late-age strength loss cannot be explained by the modest increase in porosity alone and instead indicates an activation-imbalance regime in which finite alkali availability is competitively consumed by silica dissolution, suppressing sustained calcium-silicate coupling and late-stage carbonate dissolution-reprecipitation. At higher silica contents (30-40%), sustained silicate availability compensates for this imbalance, enabling recovery of both early-age and 21-day UCS. Overall, the non-monotonic dependence of UCS on silica flour replacement (0, 20, 30, 40%) reflects an activation-balance mechanism in which finite SMS is competitively partitioned between carbonate and silicate dissolution pathways.

In addition to this competition-controlled behavior at early and intermediate ages, late-age strength development in carbonate-rich systems can benefit from secondary calcium carbonate dissolution-reprecipitation under hydrothermal conditions (Yamasaki et al., 1993). The increase in UCS observed at 21 days in the silica-free system is consistent with continued carbonate mobility in the absence of silica competition for SMS, allowing secondary $CaCO_3$ precipitation to progressively fill pores and heal microcracks. This interpretation is supported by the corresponding decrease in porosity and indicates that late-stage carbonate cementation provides an additional strengthening mechanism distinct from silicate binder formation, highlighting the time-dependent balance between carbonate- and silicate-driven pathways.

Porosity decreases with increasing silica content at 7 days but is considerably less sensitive to silica content at 21 days, indicating that the observed strength trends cannot be explained by porosity alone. Instead, silica content primarily controls the nature and continuity of the binding phase assemblage, with a compositional threshold beyond which additional silica improves both early- and late-age mechanical integrity.

To reduce reliance on calcium carbonate as the sole structural component, mitigating excessive carbonate presence, and possible silica reprecipitation as a weak silica gel, the system was further modified with olivine partially replacing remaining calcium carbonate (Figure 4). This dramatically increased UCS from <800 psi (no olivine) to >2000 psi at 20-40% olivine. Furthermore, the strength increased for all olivine containing blends with curing time. The water demand is higher for olivine-containing slurries. This caused higher porosity than in the cements without olivine (~32% to 39% increase after 7 days and ~33 to 37% increase after 14 days for the slurry with 40% olivine in the blend). This did not prevent the strength increase. The multiphase olivine precursor acts as a slow-reacting magnesium source while simultaneously providing a rigid, thermally stable skeletal framework. Even with limited chemical transformation, this framework enhances load transfer and interfacial bonding with reaction products formed under hydrothermal alkaline conditions, explaining the substantial strength increase observed despite high residual forsterite contents. This interpretation is consistent with the stoichiometric analysis, which indicates redistribution of magnesium beyond the crystalline inventory and suggests a contribution from low-crystallinity Mg-bearing reaction products. Olivine can participate in formation of magnesium-silicate phases (Allen & Seyfried, 2003; Barnes et al., 1978), reinforcing framework and providing mechanical skeleton for other silicate binding phases as well as increasing HT structural stability of resulting composite. Although olivine reinforces the framework, it also competes for SMS, which is consumed during partial dissolution of Mg-silicates and formation of secondary magnesium phases that influence microstructure and stiffness. To increase sodium availability and shift calcium partitioning toward crystalline calcium (sodium) silicates—thereby reducing sensitivity to SMS competition—the system was further evaluated with increasing additions of SBC (Figure 5).

UCS increased strongly with SBC content, exceeding 3000 psi at 7% SBC, and continued to increase with curing time. However, the UCS response was non-monotonic: while strength increased at 3% and 7% SBC, the sample containing 5% SBC exhibited lower strength.

Porosity decreased with increasing SBC concentration up to 5% and with curing time, although this decrease was non-linear. A slight increase in porosity was observed at 7% SBC; however, this did not adversely affect UCS, indicating that porosity alone does not control mechanical performance. The effect of SBC is therefore attributed to enhanced dissolution of calcium carbonate and silicate phases and increased availability of sodium ions, which promote the formation of calcium (sodium) silicate binding phases. In this context, SBC acts not only as a carbonate source but also as a phase-directing additive that influences reaction pathways and binder connectivity. The non-monotonic strength response at intermediate SBC contents suggests competing reaction pathways and transient imbalance in sodium availability, whereas higher SBC concentrations provide sufficient sodium to stabilize continuous silicate binder formation. These mechanical trends are consistent with the phase assemblage shifts identified by XRD, particularly the increased prevalence of sodium-stabilized calcium silicate phases at higher SBC contents. Overall, the mechanical response of the system reflects a chemically regulated activation balance in which phase assemblage, elemental redistribution, and interfacial bonding exert a stronger control than total porosity alone.

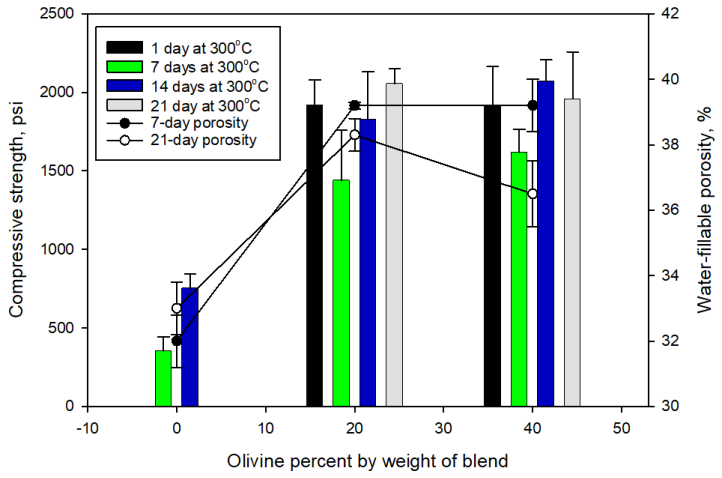

Figure 4: Effect of calcium carbonate replacement with olivine on unconfined compressive strength (UCS) of calcium carbonate /silica flour samples (60/40 wt.% blend) activated with 10% by weight of blend sodium-meta-silicate after different autoclave curing times at 300°C.

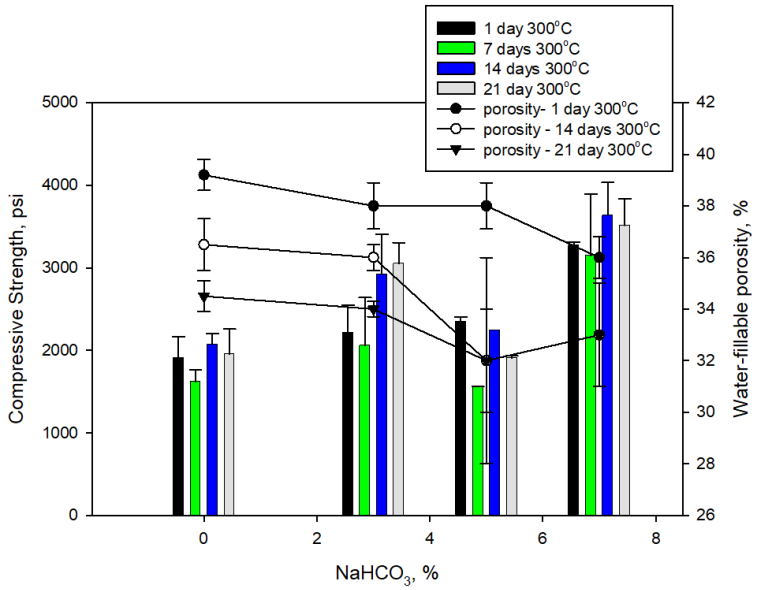

Figure 5: Effect of SBC on unconfined compressive strength (UCS) and water-fillable porosity of calcium carbonate/silica flour/olivine samples (36/24/40 wt.%) activated with 10% by weight of blend sodium-meta-silicate after different autoclave curing times at 300°C.

3.4 Microstructural observations

Representative SEM–EDS observations were used to qualitatively assess phase persistence and reaction textures in selected formulations after 21 days of hydrothermal curing at 300 °C. These observations are intended to corroborate XRD-derived phase assemblages and

provide microstructural context for the observed mechanical behavior, rather than to establish quantitative phase distributions. SEM imaging reveals the persistence of coarse precursor-derived grains embedded within a finer-grained matrix in both sodium bicarbonate–free and sodium bicarbonate–containing systems. Based on XRD-derived phase assemblages, these coarse grains are attributed to residual calcite-, quartz-, and olivine-bearing precursor phases rather than to newly formed reaction products. In the sodium bicarbonate–free system, large coarse grains are frequently observed, consistent with incomplete carbonate consumption and retention of crystalline calcium reservoirs identified by XRD (Table 3).

Samples containing SBC exhibit more pronounced reaction textures at grain boundaries and within intergranular regions. Grain surfaces appear more chemically heterogeneous, consistent with enhanced dissolution-reprecipitation processes promoted by increased sodium availability. These qualitative differences align with the XRD-observed shift toward sodium-stabilized calcium silicate phases in bicarbonate-containing systems and with the enhanced mechanical performance observed for these formulations. Overall, the microstructural observations support the conclusions drawn from XRD and stoichiometric analyses: reaction pathways under hydrothermal alkaline conditions involve partial transformation and redistribution of precursor phases, with mechanical performance governed by interfacial bonding and phase connectivity rather than by complete precursor dissolution or bulk porosity alone.

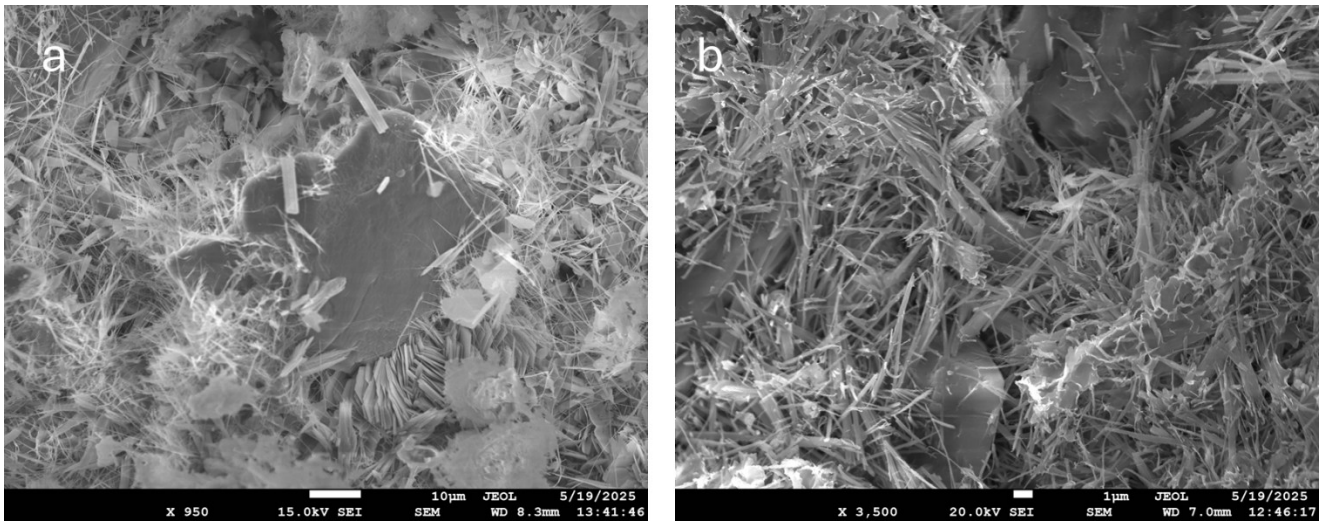

Figure 6: Representative SEM–EDS images of calcium carbonate–silica–olivine systems after 21 days of hydrothermal curing at 300 °C: (a) 0% SBC and (b) 7% SBC. Residual precursors' grains are observed in both systems, consistent with XRD-derived phase assemblages. Differences in reaction textures and grain-boundary chemistry qualitatively reflect activator-dependent reaction pathways.

CONCLUSIONS

An economic and sustainable non-clinkered CC/Si/OLV blend achieves mechanical performance above 3000 psi after 21 days at 300 °C, consistent with API recommendations for geothermal cementing applications (API technical Report 17TR8, 2011). The mechanical response reflects an activation balance in which a finite supply of SMS is consumed by carbonate, silica, and olivine reactions. UCS is lower when this competition limits coordinated Ca release and silicate availability, and higher when added SBC increases sodium availability and is associated with greater formation of Na–Ca silicate phases. Crystalline phase results indicate that activator selection is associated with systematic changes in phase assemblage: SMS provides silicate species, while Ca is supplied through alkali-driven carbonate activation together with silica dissolution; SBC tends to increase pectolite fraction and alters the persistence of lalondeite rather than implying a strictly one-way conversion. Silica flour acts as a continued source of silicate at later ages, and olivine provides a rigid mineral framework together with a gradual Mg source under hydrothermal curing. Stoichiometric analysis shows a systematic Mg/Si deficit within the quantified crystalline inventory, which is consistent with a portion of Mg residing in poorly crystalline or very fine products. The identity and mechanical role of these Mg-bearing products require further microstructural characterization. Water-fillable porosity generally decreases with curing and with SBC addition, but does not uniquely predict UCS, indicating that performance depends on the combined effects of phase assemblage, crystallinity, and interfacial bonding rather than porosity alone. Overall, these results show that non-clinkered mineral precursors can deliver strong hydrothermal performance through controlled activator chemistry and precursor proportions, while recognizing that crystalline phase quantification represents only the detected crystalline fraction and does not account for low-crystallinity products.

FUTURE WORK

Pectolite formation can produce a relatively dense microstructure and may also increase stiffness and reduce compliance, properties that are critical for thermal shock resistance in high-temperature geothermal wells. Future work should therefore evaluate system performance under thermal cycling conditions representative of geothermal operations. Thermal-cycling response is governed not only by phase assemblage but also by microstructural and morphological features, including pore connectivity and binder distribution and continuity.

High-resolution X-ray computed tomography could further elucidate the non-linear UCS response observed with SBC content, particularly the strength minimum at 5% addition, by resolving internal structural heterogeneity and damage features that are not captured by bulk porosity metrics. Ultimately, integrating these insights with cost, scalability, and deployment constraints will be essential for translating chemically designed non-clinkered cement systems into practical geothermal well applications.

ACKNOWLEDGEMENT

This work was supported by the U.S. Department of Energy, Office of Science supporting the Energy Earth-shot Initiative, as part of the "Center for Coupled Chemo-Mechanics of Cementitious Composites for EGS (C4M)" project at Brookhaven National Laboratory under contract number 2026-BNL-IS012-FUND. This research used 28-ID-1 (PDF) and 28-ID-2 (XPD) beamlines at the National Synchrotron Light Source II, a U.S. DOE Office of Science User Facility operated for the DOE Office of Science by Brookhaven National Laboratory under contract no. DE-SC0012704.

REFERENCES

Allen, D. E., & Seyfried, W. E. (2003). Compositional controls on vent fluids from ultramafic-hosted hydrothermal systems at mid-ocean ridges: An experimental study at 400 °C, 500 bars. *Geochimica et Cosmochimica Acta*, *67*(8), 1531–1542. https://doi.org/10.1016/S0016-7037(02)01173-0

API technical Report 17TR8. (2011). *High-Pressure High-Temperature Design Guidelines*.

Arbad, N., Emadi, H., & Watson, M. (2022). A comprehensive review of geothermal cementing from well integrity perspective. In *Journal of Petroleum Science and Engineering* (Vol. 217). Elsevier B.V. https://doi.org/10.1016/j.petrol.2022.110869

Barnes, I., Trescases, J. J., Pr, D., Cazadero, ny, & La Riviere Ruisseau Calif Wadi Jizi Rustaq Khafifah Coulree, L. (1978). Present day serpentinization in New Caledonia, Oman and Yugoslavia OMAN Semail ophiolite NEW CALEDONIA YUGOSLAVIA. In *Notes Geochlmlca et Cosmochimlcs Acta* (Vol. 42). Pergamon Press.

Bergen, S. L., Zemberekci, L., & Nair, S. D. (2022). A review of conventional and alternative cementitious materials for geothermal wells. *Renewable and Sustainable Energy Reviews*, *161*, 112347. https://doi.org/10.1016/j.rser.2022.112347

Coelho, A. A. (2018). TOPAS and TOPAS-Academic: An optimization program integrating computer algebra and crystallographic objects written in C++. *Applied Crystallography* , *51*, 210–218.

Devers, C., Romero Tellez, M. L., Teodoriu, C., & Amani, M. (2022). Influence of Abundant Water on Geopolymer Curing at Elevated Temperatures. *Transactions - Geothermal Resources Council*, *46*, 1452–1466.

Devers, C., Teodoriu, C., Salehi, S., & Amani, M. (2022). Geopolymers, are they consistent enough for geothermal? *47th Workshop on Geothermal Reservoir Engineering*.

Eslami, A., Malvoisin, B., Fukuyama, M., Godard, M., Ichiyama, Y., Aradi, L. E., Michibayashi, K., Wang, Z., Li, M., & Cavallo, A. (2025). Xonotlite and pectolite in rodingites from the Samail ophiolite: Markers of reducing conditions and element transfer during peridotite-gabbro interaction. *Lithos*, *512–513*. https://doi.org/10.1016/j.lithos.2025.108160

Li, N., Zhou, D., Wan, J., Zhang, Z., Jia, F., Ye, J., Zhi, X., & Chen, W. (2025). Atomic-scale insights into mechanical properties of calcium silicate hydrates: role of hydrogen bond networks and bond order distributions. *RSC Advances*, *15*(13), 10365–10377. https://doi.org/10.1039/d5ra01607j

Liu, S., Devoe, M., Samuel, D. M., Kriven, W. M., Bai, J., Ilgen, A. G., Sugama, T., & Pyatina, T. (2025). Geo-Responsive Chemomechanics in Aluminum Oxyhydroxide via Alkali-Driven Dehydroxylation for Supercritical Geothermal Systems. *ACS Materials Letters*, 1869–1878. https://doi.org/10.1021/acsmaterialslett.4c02678

Liu, S., Devoe, M., Sugama, T., Bai, J., & Pyatina, T. (2025, February 11). Elucidating the Alkali-Activated Dissolution Mechanisms in Boehmite-Based Cementitious Composites Under Enhanced Geothermal Conditions Using In-situ Synchrotron Characterization. *Proceedings, 50th Workshop on Geothermal Reservoir Engineering, Stanford University*.

Prescher, C., & Prakapenka, V. B. (2015). DIOPTAS: a program for reduction of two-dimensional X-ray diffraction data and data exploration. *High Pressure Research*, *35*, 223–230.

Pyatina, T., Sugama, T., Moghadam, A., Naumann, M., Skorpa, R., Feneuil, B., Soustelle, V., & Godøy, R. (2024). Assessment of Cementitious Composites for High-Temperature Geothermal Wells. *Materials*, *17*(6). https://doi.org/10.3390/ma17061320

Ranjbar, N., & Zhang, M. (2020). Fiber-reinforced geopolymer composites: A review. *Cement & Concrete Composite*, *107*, 103498. https://doi.org/https://doi.org/10.1016/j.cemconcomp.2019.103498

Smalakyas, G. (2021). *Peculiarities of tobermorite and xonotlite synthesis from natural rocks, their properties and applications*. http://ktu.edu

Tian, H., Stephan, D., Lothenbach, B., & Lehmann, C. (2021). Influence of foreign ions on calcium silicate hydrate under hydrothermal conditions: A review. In *Construction and Building Materials* (Vol. 301). Elsevier Ltd. https://doi.org/10.1016/j.conbuildmat.2021.124071

Yamasaki, N., Weiping, T., & Yanagisawa, K. (1993). Solidification of CaCO3 containing SrCO3 by hydrothermal hot-pressing. *Journal of Materials Research*, 1972–1976.